

## Linear ac dynamics of vortices in a periodic pinning array

Clécio C. de Souza Silva\* and J. Albino Aguiar

*Departamento de Física, Universidade Federal de Pernambuco, 50670-901 Recife-PE, Brazil*

V. V. Moshchalkov

*Nanoscale Superconductivity and Magnetism Group, Laboratorium voor Vaste-Stoffysica en Magnetism, K.U. Leuven, Celestijnenlaan, 200D Leuven, Belgium*

(Received 13 May 2003; published 7 October 2003)

The vortex-dominated ac response of a superconducting film with a periodic array of pinning centers is studied in the linear regime for vortex densities greater than the saturation number. A simple model is introduced to describe small oscillations of the vortex lattice, which is considered to be composed of two distinct lattices formed by trapped vortices and interstitial vortices. The frequency-dependent complex resistivity is calculated as a function of frequency and magnetic induction for vortex densities between the first and the second matching fields. It is shown that the absorption spectra has two peaks corresponding to two characteristic pinning frequencies: one due to the periodic pinning array and another due to vortex-cage pinning. The range of validity of the model is determined from direct numerical simulations.

DOI: 10.1103/PhysRevB.68.134512

PACS number(s): 74.25.Qt, 74.78.Na, 74.25.Nf, 74.25.Fy

### I. INTRODUCTION

Measurements of the response to ac magnetic fields or currents in type-II superconductors have been widely used to study the dynamics and pinning properties of the vortex lattice (VL) in the mixed state. Such experiments are aimed at testing theories of vortex phases in the presence of quenched disorder,<sup>1,2</sup> surface pinning,<sup>3</sup> columnar defects produced by heavy-ion irradiation,<sup>4</sup> and, more recently, nanoengineered periodic pinning arrays.<sup>5</sup>

For specimens with random point defects as the main source of pinning, the linear response is usually well accounted for by a single-particle model,<sup>6,7</sup> which describes small oscillations of vortices by the equation of motion

$$\eta \dot{u} = -\alpha_L u + F_{ac}(t), \quad (1)$$

where  $u$  is the displacement from the local minimum,  $\alpha_L$  is the phenomenological spring constant of the pinning potential (usually referred to as the Labusch constant),  $\eta$  is the viscous drag coefficient,  $F_{ac}(t) = \phi_0 J_{ac}(t)$  is the Lorentz force due to a small ac current density  $J_{ac}(t) = J e^{-i\omega t}$ , and  $\phi_0 = h/2e$  is the quantum flux. The well-known steady-state solution for Eq. (1),  $u(t) = u(\omega) e^{-i\omega t}$ , where  $u(\omega) = \phi_0 J / (-i\eta\omega + \alpha_L)$ , leads to a complex, frequency dependent resistivity,  $\rho_{ac}(\omega) = \dot{u}(t) B / J_{ac}(t) = -i\omega u(\omega) B / J$ . By taking the Bardeen-Stephen value for the friction coefficient,  $\eta = \phi_0 B c_2 / \rho_n$ , where  $\rho_n$  is the normal-state resistivity, one finds

$$\rho_{ac}(\omega) = \rho'(\omega) - i\rho''(\omega) = \frac{\omega^2 - i\omega\omega_L}{\omega^2 + \omega_L^2} \rho_{FF}, \quad (2)$$

where  $\omega_L = \alpha_L / \eta$  and  $\rho_{FF} = (B/B_{c2})\rho_n$  is the flux-flow resistivity. For nonzero temperatures, the possibility of creep phenomena should be taken into account.<sup>8</sup> Nevertheless, for strong pinning, the effect of creep is negligible except for very low frequencies. This single-particle model is in agree-

ment with many experiments in a broad range of frequencies, fields, and temperatures on low- and high- $T_c$  bulk materials, where the phenomenological Labusch constant is a statistical average over some single peaked distribution of restoring forces.<sup>9</sup>

For superconducting films with periodic arrays of pinning centers a different scenario takes place. To be specific, let us assume that each center can pin only one single-quantum vortex, i.e., the saturation number of the pinning array is  $n_s = 1$ . For fields below or equal to the first matching field  $B_1$ , all vortices are trapped by the artificial pinning centers.<sup>10</sup> If the vortices form a perfect lattice, as in the case of the submatching fields ( $B/B_1 = 1/4, 1/3, 1/2$ , etc.), the single-particle model may be applied very successfully and the obtained Labusch constant will be a very precise measure of the individual pinning strength produced by artificial traps. Once the pinning array is saturated, the additional vortices occupy the interstitial positions in the superconducting matrix and are caged through the interactions with the vortices strongly pinned by the artificial traps. In this case we are dealing with two different pinning potentials acting on two different vortex species, and the one-particle model seems to break down.

In this work we propose a simple model to study the linear ac response of a vortex lattice in superconducting films with a periodic array of pinning centers for vortex densities above the saturation number. We propose that this composite vortex lattice, composed of a strongly pinned sublattice and a weakly caged interstitial one, has two main characteristic ‘‘pinning’’ frequencies: one due to the coupling between the vortex lattice and the periodic matrix and another due to the coupling between the two sublattices. We also assume that these two sublattices are rigid, which reduces the problem to a two-particle one. The calculated frequency-dependent ac response is strikingly distinct from that obtained by a simple one-particle model. For instance, the imaginary part of the ac resistivity has, for strong pinning, a double peak, featuring the two frequency modes. A direct comparison with numerical simulations shows that the two-particle model well de-

scribes the ac response for fields  $B_1 \leq B \leq 2B_1$ . For higher vortex densities, internal modes of the interstitial vortex lattice become important and the assumption of rigid lattice is not valid any longer.

## II. A TWO-SPECIES MODEL

We consider the dynamics of  $N$  point vortices in a two-dimensional superconducting system with a periodic array of pinning centers. The vortices are assumed to be massless particles obeying the overdamped equation of motion

$$\eta \dot{\mathbf{r}}_i = - \sum_{j \neq i}^N \nabla_i V(r_{ij}) - \nabla U_p(\mathbf{r}_i) + \phi_0 \mathbf{J}_{ac}(t) \times \hat{z}, \quad (3)$$

where  $V(r_{ij})$  is the vortex-vortex interaction potential,  $U_p(\mathbf{r}_i)$  is the pinning potential representing the effect of the periodic pinning array, and  $r_{ij} = |\mathbf{r}_i - \mathbf{r}_j|$ . Usually, for field values higher than the first matching field, the interstitial vortices order into a commensurate lattice at matching or fractional matching fields or arrange themselves into domains of ordered lattices<sup>11</sup> in nonmatching fields. Here we shall consider only the cases where the interstitial vortices form a commensurate lattice, in such a way that the forces on a interstitial vortex due to other interstitial vortices are canceled out due to the symmetry. Thus, we have two distinct, well defined vortex lattices: one *pinned* by the periodic pinning array and the other one is the *caged interstitial* vortex lattice. Pinned vortices will be referred to as species-*A* vortices and interstitial vortices will be referred to as species-*B* vortices. We further assume that, for small uniform driving forces, the lattices move with respect to each other as rigid bodies.

For small excitations, vortices of species *A* are elastically connected to the sample due to the periodic pinning potential, with spring constant  $\alpha_p$  and those of species *B* are elastically connected to the pinned-vortex lattice via vortex-vortex interactions, with spring constant  $\alpha_v$ . This problem is analogous to the mechanical problem of two massless blocks, representing the sublattices *A* and *B*, connected to each other by a spring, one of them (block *A*) being connected to a wall, which here represents the superconducting sample. The spring connecting the two blocks has an effective elastic constant  $N_B \alpha_v$ , where  $N_B$  is the total number of caged interstitial vortices, and the one connecting block *A* to the wall has an effective elastic constant  $N_A \alpha_p$ , where  $N_A$  is the number of pinned vortices (which coincides with the number of pins). This is schematically represented in Fig. 1, where we also show a vortex lattice at the second matching field being deformed by a uniform force [Fig. 1(a)]. Note that the forces acting on lattices *A* and *B* are  $N_A F$  and  $N_B F$ , respectively. Thus, for a small ac drive, we can reduce the set of  $N$  coupled equations, given by Eq. (3), to a set of two linear equations, each one describing the motion of the center of mass of one sublattice:

$$\eta \dot{u}_A = -\alpha_p u_A - n_B \alpha_v (u_B - u_A) + \phi_0 J_{ac}(t), \quad (4)$$

$$\eta \dot{u}_B = -\alpha_v (u_A - u_B) + \phi_0 J_{ac}(t), \quad (5)$$

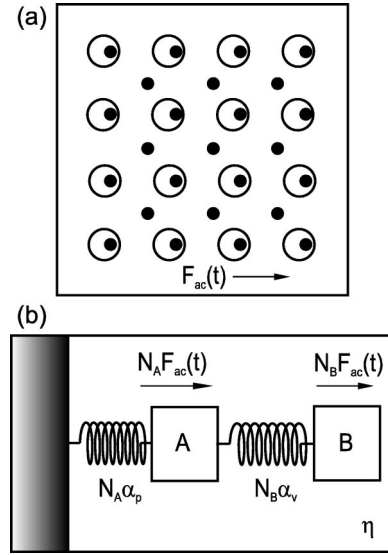


FIG. 1. (a) Vortex lattice (full circles) at the second matching field deformed from its equilibrium configuration by a uniform force. The hollow circles represent the artificial traps. (b) Schematic representation of the mechanical analog: block *A* represents the pinned vortex array, which is elastically coupled to the superconducting sample, and block *B* represents the interstitial vortex array, which is elastically coupled to the pinned-vortex array (see text).

where  $n_B = N_B/N_A$  is the occupation number of interstitial vortices. The solution for this linear system is  $u_A(t) = u_A(\omega) e^{-i\omega t}$  and  $u_B(t) = u_B(\omega) e^{-i\omega t}$ , with

$$u_A(\omega) = \frac{n \omega_v - i \omega}{\omega_v \omega_p - \omega^2 - i \omega (n \omega_v + \omega_p)} \frac{\phi_0 J}{\eta}, \quad (6)$$

$$u_B(\omega) = \frac{n \omega_v + \omega_p - i \omega}{\omega_v \omega_p - \omega^2 - i \omega (n \omega_v + \omega_p)} \frac{\phi_0 J}{\eta}. \quad (7)$$

Here,  $n = (N_A + N_B)/N_A = B/B_1$  is the total occupation number,  $\omega_p = \alpha_p/\eta$ , and  $\omega_v = \alpha_v/\eta$ . With this solution one can easily calculate the complex resistivity of the vortex system,  $\rho_{ac}(\omega) = v(t)B/J_{ac}(t)$ , by noting that the center of mass velocity  $v$  is  $-i\omega u(t)$ , where  $u(t) = (N_A u_A + N_B u_B)/N$ . The resistivity is then given by

$$\rho_{ac}(\omega) = \frac{-\omega^2 + i \omega \left( n \omega_v + \frac{n_B}{n} \omega_p \right)}{\omega_v \omega_p - \omega^2 + i \omega (n \omega_v + \omega_p)} \rho_{FF}. \quad (8)$$

Thus, the overall linear ac response of the vortex system can be completely determined by two characteristic frequencies: the pinning frequency  $\omega_p$  and the ‘‘vortex-cage’’ frequency  $\omega_v$ .

Another important physical quantity is the ac penetration depth  $\lambda_{ac}$ . By using London's equation  $\mathbf{E} = \mu_0 \partial(\lambda^2 \mathbf{J})/\partial t$ , one can easily relate  $\lambda_{ac}$  to the complex resistivity,  $\rho_{ac}(\omega) = E(t)/J(t)$ . Since  $E(\omega) = v(\omega)B = -i\omega u(\omega)B$ , where  $u(\omega) = [N_A u_A(\omega) + N_B u_B(\omega)]/N$  and  $u_A(\omega)$  and  $u_B(\omega)$  are given by Eqs. (6) and (7), we have

$$\lambda_{ac}^2(\omega) = \frac{\rho_{ac}(\omega)}{-i\omega\mu_0} = \frac{B}{\mu_0 J} u(\omega), \quad (9)$$

which is proportional to the complex oscillation amplitude of the center of mass,  $u(\omega)$ .

The vortex-cage frequency  $\omega_v$  is determined by the vortex-vortex interactions and can be calculated for a particular vortex distribution by considering a specific vortex-vortex potential. Here we consider Pearl vortices in a thin film (with thickness  $d \ll \lambda$ ) with the pair potential

$$V(r) = \int \frac{d^2k}{4\pi^2} \tilde{V}(k) e^{i\mathbf{k}\cdot\mathbf{r}},$$

where  $\tilde{V}(k) = 2\pi\epsilon/(k^2 + 2\Lambda^{-1}k)$ ,  $\epsilon = \phi_0^2/2\pi\lambda^2$  is the energy scale, and  $\Lambda = \lambda^2/d$  is the effective penetration depth. The potential generated by the square lattice of pinned vortices may be written as a Fourier expansion

$$U_v(x,y) = 2\pi\epsilon \sum_{\mathbf{G}} \frac{e^{i\mathbf{G}\cdot\mathbf{r}} F(G)}{G^2 + 2\Lambda^{-1}G}, \quad (10)$$

where  $\mathbf{G} = 2\pi/a_p(m,n)$  are reciprocal lattice vectors of the pinned VL ( $a_p$  is the pinning periodicity) and  $F(G)$  is the cutoff function necessary to eliminate the divergencies and account for the vortex core.<sup>12</sup> In the high-density limit ( $a/\pi \ll \Lambda$ ), the vortex-vortex interaction is essentially logarithmic,  $V(r) = \epsilon \ln(r)$ , and the lattice sum in Eq. (10) can be written as a rapidly converging series.<sup>13,14</sup> For a square lattice one finds

$$U_v(x,y) = C + \epsilon\pi \frac{y^2}{a_p^2} - \frac{\epsilon}{2} \sum_{k=-\infty}^{\infty} \ln \frac{\cosh 2\pi \left( \frac{y}{a_p} + k \right) - \cos \frac{2\pi x}{a_p}}{\cosh 2\pi k}, \quad (11)$$

where  $C$  is a constant depending on system size. This potential has minima at  $(x,y) = a_p/2(m,n)$ . The spring constant for a single interstitial vortex located in a minimum of this potential corresponds to the second derivative of  $U_v$  evaluated at this point. The result is

$$\alpha_v = \frac{2\pi^2\epsilon}{a_p^2} \sum_{k=-\infty}^{\infty} \frac{1}{1 + \cosh \pi(2k+1)} = \frac{\pi\epsilon}{a_p^2}. \quad (12)$$

### III. NUMERICAL SIMULATIONS

In order to test the predictions of the model presented in Sec. II, we have performed numerical simulations for vortices in a square pinning array. The pinning potential is modeled by a well-behaved periodic function,

$$U_p(x,y) = \frac{\pi^2\alpha_p}{a_p^2\xi_p^2} e^{-1/2(\beta_x^2 + \beta_y^2)/\xi_p^2}, \quad (13)$$

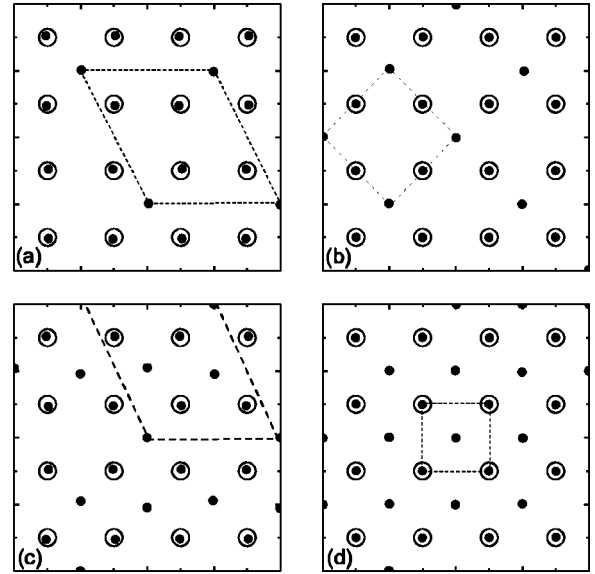


FIG. 2. Snapshots of the ground-state vortex configurations (full circles) for occupation numbers  $n = 1.25$  (a),  $1.5$  (b),  $1.75$  (c), and  $2$  (d). Open circles represent the pinning centers and dashed lines denote the unit cell of the vortex lattice.

where  $\beta_u = \sin(\pi u/a_p)$ ,  $u = x, y$ , and  $\xi_p = \sin(\pi r_p/a_p)$ . Equation (13) is normalized in such a way that  $\alpha_p$  gives the restoring force constant at a minimum of the potential. For  $r_p \ll a_p$ , this expression represents a square array of Gaussian traps and  $r_p$  coincides with the maximum pinning force radius.

We assume periodic boundary conditions in a square simulation cell of size  $L$ . The calculations were made for vortex densities ranging from  $n = 1$  to  $2$  in steps of  $1/4$ . The largest vortex lattice periodicity was  $2a_p$ . We have checked that vortices which occupy equivalent positions in the unit cell are strongly correlated when responding to a uniform external force regardless of the excitation frequency. Bearing this in mind, a system size with just a few unit cells ( $L = 4a_p$ , with  $a_p = \Lambda/4$ ) was used.

To obtain the VL ground-state configurations for a given  $n$ , we used the Monte Carlo simulated annealing method, i.e., starting from a high-temperature molten state, we minimize the free energy by slowly decreasing the temperature. Some of these ground-state configurations are shown in Fig. 2 and are essentially the same as those obtained in earlier numerical calculations.<sup>15</sup>

The VL ac response to an oscillating current was calculated by molecular-dynamics simulations. We start with the ground-state configurations obtained by the Monte Carlo annealing and then numerically integrate the equations of motion [Eq. (3)] as a small oscillating current is applied. To study the possibility of anisotropic response we choose  $\mathbf{J}_{ac}(t) = J e^{-i\omega t} (\hat{x} - i\hat{y})/\sqrt{2}$ , that is, a rotating current with out-of-phase  $x$  and  $y$  components and constant modulus  $J$ . For  $B_1 \leq B \leq 2B_1$  we have found that the linear response is rather isotropic, i.e., the VL center of mass describes circular orbits. This means that the pinning and vortex-cage couplings are determined by a single isotropic elastic constant.

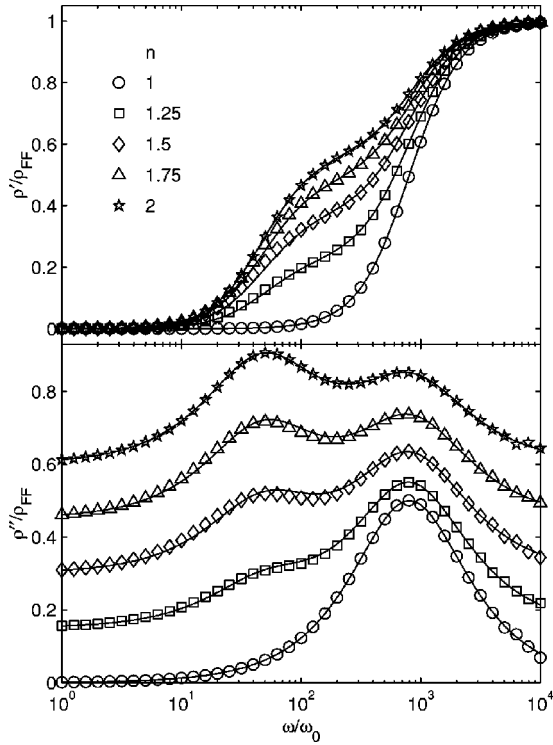


FIG. 3. Real  $\rho'$  (top panel) and imaginary  $\rho''$  (bottom panel) parts of the ac resistivity for a square pinning array with periodicity  $a_p = \Lambda/4$  and pinning strength  $\alpha_p = 16\pi\epsilon/a_p^2$ . The open symbols are results from the simulations described in Sec. III for  $n = B/B_1 = 1$  ( $\circ$ ), 1.25 ( $\square$ ), 1.5 ( $\diamond$ ), 1.75 ( $\triangle$ ), and 2 ( $\star$ ). The full lines are plots of Eq. (8) for these field values. No fitting parameter is used. The data for the imaginary resistivity are offset for a better visualization.

#### IV. RESULTS AND DISCUSSION

The simulations were performed for a frequency range of four decades. For each frequency we calculated the complex resistivity, which is given by  $\rho = (B/J)(1/N)\sum_{i=1}^N \dot{r}_i$ . The data for  $n = 1, 5/4, 3/2, 7/4, \text{ and } 2$  are plotted in Fig. 3. The pinning parameters used are  $\alpha_p = 16\pi\epsilon/a_p^2$ ,  $a_p = 0.25\Lambda$ , and  $r_p = 0.1a_p$ . The frequency scale is given by  $\omega_0 = \epsilon/\eta\Lambda^2$ . In this figure we also show the analytical frequency-dependent resistivity [Eq. (8)] calculated using the same pinning parameters and  $\alpha_v$  given by Eq. (12). For this strong pinning strength, the lines fit the numerical data very well (note that no fitting parameter was used).

We also performed simulations for vortex densities close to the (fractional) matching fields considered here. These vortex densities correspond to adding or removing one vortex (per simulation cell) in the vortex lattices presented in Fig. 2. The resulting vortex lattices present low symmetry in comparison with those corresponding to fractional matching configurations. Although the two-species model is based on severe symmetry restrictions, we observed that the ac response of these low-symmetry vortex arrangements follow the model predictions quite well. These results suggest that for strong pinning, the response predicted by the two-species model are expected to hold in the entire field range between the first and the second matching fields. For vortex densities

slightly greater than  $n=2$ , the response is qualitatively different from the model prediction, although the main features predicted by the model are kept. In this case, an additional vortex combine with an interstitial one to form a vortex dimer. This dimer introduces a new vortex species with its own elastic properties, which are not considered in the model.

For weaker pinning strengths we observed that the agreement between the two-species model and the simulations is poor at fractional or nonmatching fields. The divergence is more critical at low frequencies, where the interstitial pinning plays an important role in the dynamics.

The complex resistivity provides little information about the vortex dynamics at low frequencies, since in this region its real and imaginary parts vanish. On the other hand, the complex penetration depth is an experimentally accessible quantity, which provides important information about the low-frequency region. In the single-particle model this length tends to the well-known Campbell penetration depth,  $\lambda_C = \sqrt{\phi_0 B/\mu_0 \alpha_L}$ , in the zero-frequency limit. (This indicates that for small enough excitations the vortex system allows penetration of additional fields only over the length  $\lambda_C$  resembling the Meissner state.) Here we can obtain a similar expression by noting that the zero-frequency center-of-mass amplitude is  $u(\omega \rightarrow 0) = \phi_0 J/\alpha_L^{\text{eff}}$ , where

$$\alpha_L^{\text{eff}} = \frac{n\alpha_v\alpha_p}{n^2\alpha_v + n_B\alpha_p} \quad (14)$$

is the effective Labusch constant. This expression can be derived with the help of Eqs. (6) and (7) or by a simple force balance analysis. Using Eq. (9) we have

$$\lambda_C^2 \equiv \lambda_{ac}^2(\omega \rightarrow 0) = \frac{\phi_0 B}{\mu_0 \alpha_L^{\text{eff}}}. \quad (15)$$

In this way, by measuring the Campbell penetration depth in the field range  $B_1 \leq B \leq 2B_1$ , one can experimentally estimate both  $\alpha_p$  and  $\alpha_v$ .

In Fig. 4, we show the real part of  $\lambda_{ac}^2$  as a function of the pinning strength  $\alpha_p$  at a low-frequency  $\omega = \omega_0$  (top panel), at the vortex-cage frequency  $\omega = \omega_v$  (center panel), and at a high-frequency  $\omega = 8\omega_v$  (bottom panel). At the second matching field we have an excellent agreement with the two-species model in the full pinning strength and frequency range. For the fractional matching fields, good agreement is achieved for high frequencies. Nevertheless, for low frequency the validity of the two-species model is restricted to strong pinning.

It is interesting to determine the contributions to  $\lambda_C$  coming from the pinned VL and the interstitial VL. First, we note that

$$\lambda_{ac}^2(\omega) = [N_A \lambda_{ac(A)}^2(\omega) + N_B \lambda_{ac(B)}^2(\omega)]/N,$$

where  $\lambda_{ac(A)}^2(\omega) = (B/\mu_0 J)u_A(\omega)$  and  $\lambda_{ac(B)}^2(\omega) = (B/\mu_0 J)u_B(\omega)$ . Then, using Eqs. (6) and (7), the zero-frequency limit for the pinned vortices is

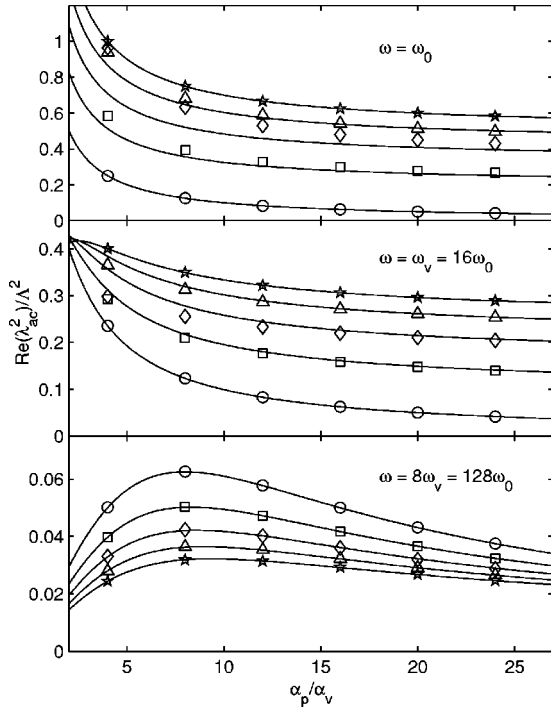


FIG. 4. Real part of the ac penetration depth  $\lambda_{ac}$  as a function of  $\alpha_p$  for different frequency regimes (from top to bottom,  $\omega = \omega_0$ ,  $\omega_v$ , and  $8\omega_v$ ). The symbols have the same meaning as in Fig. 3 and are compared to the corresponding two-species model prediction (full lines), i.e., Eq. (9).

$$\lambda_{C(A)}^2 = (B/\mu_0 J)u_A(0) = \phi_0 B/\mu_0 \alpha_A,$$

where  $\alpha_A = \alpha_p/n$  and for the interstitial vortices is  $\lambda_{C(B)}^2 = \phi_0 B/\mu_0 \alpha_B$ , where  $\alpha_B = \alpha_v \alpha_p / (n \alpha_v + \alpha_p)$ . Note that for  $\alpha_p \gg \alpha_v$ ,  $\alpha_B \approx \alpha_v$  and the contribution of the interstitial vortices to the Campbell penetration depth is much larger than the contribution from the pinned vortices, as expected.

In Fig. 5, we plot the real and imaginary parts of the contributions of the pinned VL (pentagrams) and the interstitial VL (lozenges) to the ac penetration depth (top panel) and the ac resistivity (bottom panel) for  $B = 2B_1$ . The lines are obtained from Eqs. (8) and (9). The ac penetration depths are normalized by their corresponding zero-frequency limit:  $\lambda_{C(A)}$  for the pinned VL and  $\lambda_{C(B)}$  for the interstitial VL. Three dynamical regimes are indicated. In the flux-flow regime ( $\omega > \omega_p$ ) the viscous drag force dominates over the pinning forces. Both pinned and interstitial VL behave as free lattices and the superconducting sample mimics the response of a normal metal with resistivity  $\rho_{FF}$  and skin depth  $\delta = \sqrt{2\rho_{FF}/\mu_0\omega}$  [in this case,  $\lambda_{ac}^2(\omega) = i\delta^2/2$  is purely imaginary].<sup>8,9</sup> For  $\omega_v < \omega < \omega_p$ , the vortex dynamics is dominated by the PPA. Here the vortices in the pinning centers are strongly pinned. As the frequency is diminished from  $\omega = \omega_p$ , the real part of  $\rho_{ac(A)}$  decreases fast, whereas the real part of  $\lambda_{ac(A)}^2$  increases indicating that the pinned-vortex response is dominated by screening. Nevertheless, the interstitial vortices seem to remain in the flux-flow regime and their response is still dissipative. At low frequencies,  $\omega$

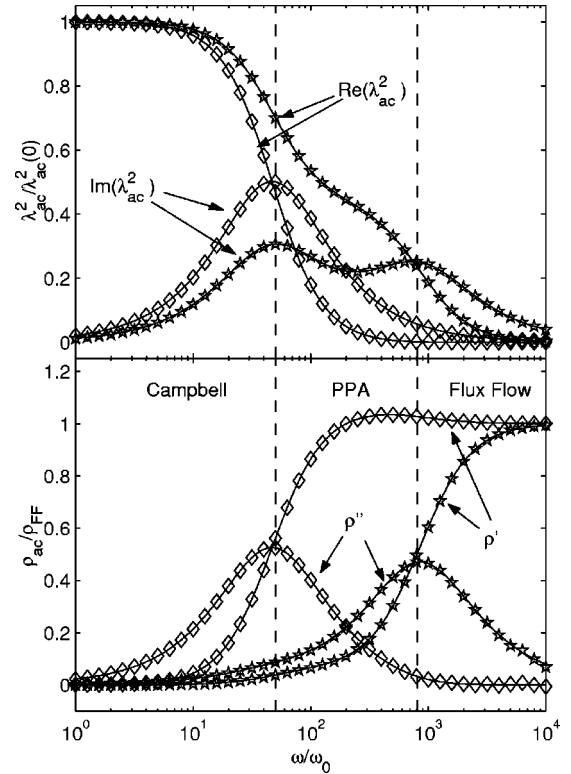


FIG. 5. Partial contributions of the pinned vortex lattice ( $\star$ ) and the interstitial vortex lattice ( $\diamond$ ) to the ac penetration depth (top) and ac resistivity (bottom) for  $B = 2B_1$ . The penetration depths are normalized by their zero-frequency value. The dashed lines indicate the characteristic frequencies  $\omega_v$  (left) and  $\omega_p$  (right), which define three different dynamical regimes: the low-frequency (quasistatic) Campbell regime, where the response is dominated by the elastic forces, the high-frequency regime, where the dynamics is dominated by the viscous drag force (flux-flow), and the intermediate frequency regime, where the dynamics is dominated by the periodic pinning array (PPA).

$< \omega_v$ , the dynamics is in the quasistatic (or Campbell) regime, which is characterized by zero resistivity and real penetration length. Both in-site and interstitial vortices are strongly pinned and the whole system behaves as in the Meissner state.

## V. CONCLUSIONS

We have proposed a simple two-species model to describe the ac dynamics of the vortex lattice in a periodic pinning array near equilibrium. This model provides solutions for small oscillations of both pinned and interstitial vortices. We have shown by direct molecular dynamics simulations that this model is a good approximation for flux densities between the first and the second matching fields. Although the mobility of the pinned vortices is, in general, much smaller than the mobility of the interstitial vortices, both vortex species have an important role in the overall dynamics. The frequency spectrum of the complex resistivity reveals two absorption peaks near the pinning  $\omega_p$  and

vortex-cage  $\omega_v$  frequencies. These peaks are more pronounced for  $B = 2B_1$ .

The results shown in this paper should be experimentally verified for superconducting films with periodic pinning arrays. The frequency spectrum should be accessible to a broadband phase-sensitive equipment. For low-frequency measurements, estimations of  $\alpha_p$  and  $\alpha_v$  may be obtained by measuring the Campbell penetration depth in the field range  $B_1 \leq B \leq 2B_1$  and using Eq. (14).

## ACKNOWLEDGMENTS

We would like to thank A.V. Silhanek for helpful discussions. C.C.S.S. and J.A.A. acknowledge the support from the Brazilian agencies FACEPE, CNPq, and CAPES. C.C.S.S. also wishes to acknowledge the hospitality of the VSM laboratory at the K. U. Leuven. V.V.M. acknowledges the support from the Flemish GOA and FWO programs, and the ESF VORTEX program.

\*Electronic address: clecio@df.ufpe.br

- <sup>1</sup>J. Kötzler, M. Kaufmann, G. Nakielski, R. Behr, and W. Assmus, Phys. Rev. Lett. **72**, 2081 (1994); J. Kötzler, G. Nakielski, M. Baumann, R. Behr, F. Goerke, and E.H. Brandt, Phys. Rev. B **50**, 3384 (1994).
- <sup>2</sup>W. Henderson, E.Y. Andrei, M.J. Higgins, and S. Bhattacharya, Phys. Rev. Lett. **80**, 381 (1998).
- <sup>3</sup>N. Lütke-Entrup, B. Plaçais, P. Mathieu, and Y. Simon, Phys. Rev. Lett. **79**, 2538 (1997); A. Pautrat, C. Goupil, C. Simon, N. Lütke-Entrup, B. Plaçais, P. Mathieu, Y. Simon, A. Rykov, and S. Tajima, Phys. Rev. B **63**, 054503 (2001).
- <sup>4</sup>G. Pasquini, L. Civale, H. Lanza, and G. Nieva, Phys. Rev. B **59**, 9627 (1992); Phys. Rev. B **65**, 214517 (2002).
- <sup>5</sup>A.V. Silhanek, S. Raedts, M. Lange, and V.V. Moshchalkov, Phys. Rev. B **67**, 064502 (2002).
- <sup>6</sup>J.I. Gittleman and B. Rosenblum, Phys. Rev. Lett. **16**, 734 (1966).
- <sup>7</sup>A.M. Campbell, J. Phys. C **2**, 1492 (1969); A.M. Campbell and J.E. Evetts, Adv. Phys. **21**, 199 (1972).
- <sup>8</sup>E.H. Brandt, Rep. Prog. Phys. **58**, 1465 (1995).
- <sup>9</sup>C.J. van der Beek, V.B. Geshkenbein, and V.M. Vinokur, Phys. Rev. B **48**, 3393 (1993).
- <sup>10</sup>M. Baert, V.V. Metlushko, R. Jonckheere, V.V. Moshchalkov, and Y. Bruynseraede, Phys. Rev. Lett. **74**, 3269 (1995); K. Harada, O. Kamumura, H. Kasai, T. Matsuda, A. Tonomura, and V.V. Moshchalkov, Science **271**, 1393 (1996); V. V. Moshchalkov, V. Bruyndocx, L. Van Look, M. J. Van Bael, Y. Bruynseraede, and A. Tonomura, in *Handbook of Nanostructured Materials and Nanotechnology*, Electrical Properties, Vol. 3, edited by H. S. Nalwa (Academic, San Diego, 2000).
- <sup>11</sup>C. Reichhardt, J. Groth, C.J. Olson, Stuart B. Field, and Franco Nori, Phys. Rev. B **54**, 16 108 (1997).
- <sup>12</sup>J.R. Clem, J. Low Temp. Phys. **18**, 427 (1975).
- <sup>13</sup>M. Doria, Physica C **178**, 51 (1991).
- <sup>14</sup>N. Grønbech-Jensen, Int. J. Mod. Phys. C **7**, 873 (1996); Comput. Phys. Commun. **119**, 115 (1999).
- <sup>15</sup>C. Reichhardt, C.J. Olson, and F. Nori, Phys. Rev. B **57**, 7937 (1998).